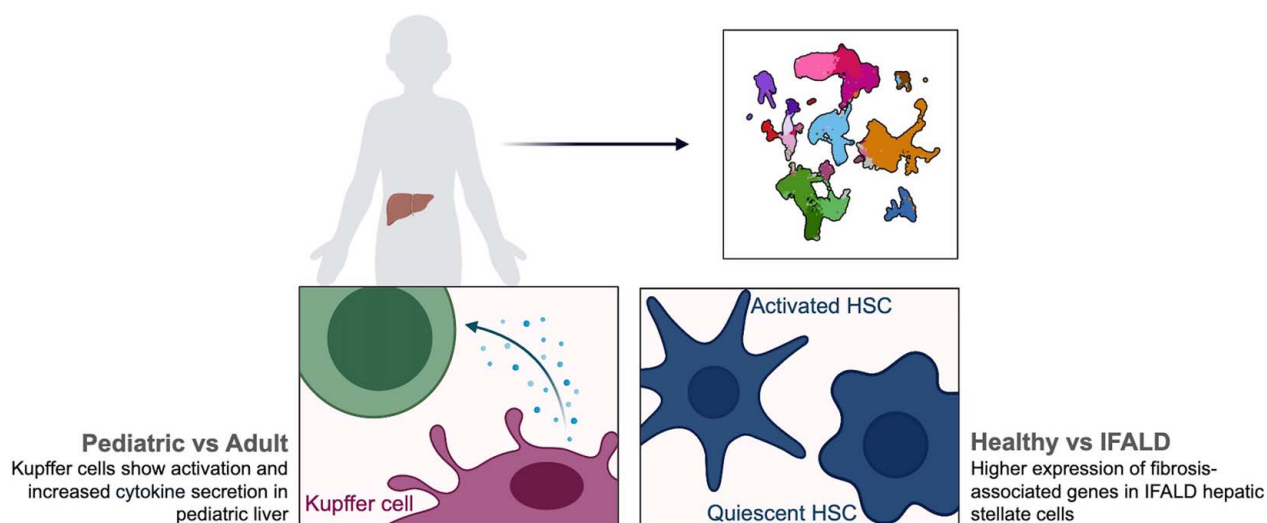


Single-cell atlas of human pediatric liver reveals age-related hepatic gene signatures

VISUAL ABSTRACT

Single-cell atlas of human pediatric liver reveals age-related hepatic gene signatures



















Created with BioRender

ORIGINAL ARTICLE

OPEN

Single-cell atlas of human pediatric liver reveals age-related hepatic gene signatures

Rachel D. Edgar^{1,2}  | Diana Nakib^{1,3}  | Damra Camat^{1,3}  | Sai Chung^{1,3}  |
 Patricia Lumanto¹  | Jawairia Atif^{1,3}  | Catia T. Perciani^{1,3}  | Xue-Zhong Ma¹ |
 Cornelia Thoeni⁴  | Nilosa Selvakumaran⁵  | Justin Manuel¹ | Blayne Sayed¹  |
 Koen Huysentruyt^{5,6}  | Amanda Ricciuto⁵  | Ian McGilvray¹  |
 Yaron Avitzur⁵  | Gary D. Bader^{2,7,8,9,10,11}  | Sonya A. MacParland^{1,3,4} 

¹Ajmera Transplant Centre, Toronto General Research Institute, University Health Network, Toronto, Ontario, Canada

²Donnelly Centre, University of Toronto, Toronto, Ontario, Canada

³Department of Immunology, University of Toronto, Toronto, Ontario, Canada

⁴Department of Laboratory Medicine and Pathobiology, University of Toronto, Toronto, Ontario, Canada

⁵Division of Gastroenterology, Hepatology & Nutrition, Hospital for Sick Children, University of Toronto, Toronto, Ontario, Canada

⁶Brussels Centre for Intestinal Rehabilitation in Children, UZ Brussel, Vrije Universiteit Brussel, Brussels, Belgium

⁷Department of Molecular Genetics, University of Toronto, Toronto, Ontario, Canada

⁸Princess Margaret Cancer Centre, University Health Network, Toronto, Ontario, Canada

⁹Department of Computer Science, University of Toronto, Toronto, Ontario, Canada

¹⁰Lunenfeld-Tanenbaum Research Institute, Sinai Health System, Toronto, Ontario, Canada

¹¹CIFAR Multiscale Human Program, CIFAR, Toronto, Ontario, Canada

Correspondence

Rachel D. Edgar, Ajmera Transplant Centre,
 Toronto General Research Institute, Address:
 585 University Avenue, Toronto, Ontario, M5G
 2N2.
 Email: r.edgar@utoronto.ca

Yaron Avitzur, Division of Gastroenterology,
 Hepatology and Nutrition, SickKids Hospital,
 Address: 555 University Ave, Toronto, ON M5G
 1X8.
 Email: aron.avitzur@sickkids.ca

Gary D. Bader, Donnelly Centre, University of
 Toronto, Address: 160 College St, Toronto,
 Ontario, M5S 3E1.
 Email: gary.bader@utoronto.ca

Abstract

Background: The liver plays a critical role in metabolism and immune function, yet the contributions of its heterogeneous cell types to these processes remain unclear. While most liver studies focus on adults, pediatric liver diseases often present differently, underscoring the need for age-specific research.

Methods: To better understand cellular drivers of childhood liver diseases, we generated single-cell RNA-sequencing maps of the normal pediatric liver and used this map to examine disease-related populations in biopsies from pediatric patients with intestinal failure-associated liver disease (IFALD).

Abbreviations: cDC1, conventional type 1 dendritic cells; GRCh38, Genome Reference Consortium Human Build 38; IFALD, intestinal failure-associated liver disease; LPS, lipopolysaccharide; MASH, metabolic dysfunction-associated steatohepatitis; Mono-Mac, Monocyte-like Macrophages; REB, Research Ethics Board; rPCA, robust principal component analysis; scRNA-seq, single-cell RNA sequencing.

Rachel D. Edgar, Diana Nakib, and Damra Camat are co-first authors.

Yaron Avitzur, Gary D Bader, and Sonya A. MacParland are co-senior authors.

Supplemental Digital Content is available for this article. Direct URL citations are provided in the HTML and PDF versions of this article on the journal's website, www.hepcommjournal.com.

This is an open access article distributed under the terms of the Creative Commons Attribution-Non Commercial-No Derivatives License 4.0 (CCBY-NC-ND), where it is permissible to download and share the work provided it is properly cited. The work cannot be changed in any way or used commercially without permission from the journal.

Copyright © 2025 The Author(s). Published by Wolters Kluwer Health, Inc. on behalf of the American Association for the Study of Liver Diseases.

Sonya A. MacParland, Ajmera Transplant Centre, Toronto General Research Institute, Address: 585 University Avenue, Toronto, Ontario, M5G 2N2.
Email: s.macparland@utoronto.ca

Results: The normal pediatric liver map consists of 42,660 cells from 9 donors under 17 years of age. Compared with normal adult liver (26,372 cells; 7 donors, age 26–69), pediatric livers exhibited differences in myeloid populations. Specifically, pediatric Kupffer-like cells (*MARCO+C1QA+VSIG4+*) exhibited higher expression of immune activation genes, including *CCL4*, *CCL3*, and *IL1B*. In vitro stimulation confirmed more IL-1 β -secreting myeloid cells in pediatric versus adult livers, supporting these findings. Using the pediatric atlas as a reference, we analyzed 3 IFALD biopsies (11,969 cells; 3 donors, under 9 y of age) and identified increased expression of fibrosis-associated genes (eg, *LY96*) in Kupffer-like cells. In addition, mesenchymal cells in IFALD showed fibrotic gene modules resembling adult liver cells more than healthy pediatric cells. These signatures, undetectable when comparing IFALD to adult liver alone, highlight the value of a pediatric map.

Conclusion: Taken together, our healthy pediatric liver atlas reveals distinct age-related signatures and provides a background against which to interpret pediatric liver disease data.

Keywords: HSCs, KC, liver zonation, single-cell transcriptomics, spatial transcriptomics

INTRODUCTION

The liver is vital for human metabolism and immune function. Although the liver is composed of a heterogeneous mix of cell types, how these cell types contribute individually, and in concert, toward liver function remains poorly understood. What is known about healthy liver function, cellular heterogeneity, and cell structures is primarily based on studies of the fetal and adult liver.^[1–8] However, there are few studies that have examined the pediatric liver with single-cell transcriptomics.^[9,10] The pediatric window is a potentially unique time in liver biology. The body's immune system is seeded in part from the fetal liver. Subsequently, populations of tissue-resident immune cells undergo tissue-specific maturation programs. How the pediatric liver resident immune system matures and differs from both the fetal liver and the fully developed adult liver is unclear.

It is well established that functional differences between pediatric and adult liver exist at the level of metabolism and response to liver damage. For example, there are differences in drug metabolism,^[11] potentially through differences in cytochrome P450 protein levels,^[12] as well as differences in ALT levels, which are an indicator of the response to liver damage.^[13] These differences in healthy liver function provide a clear rationale for creating an atlas focused on pediatric livers. Furthermore, there are liver diseases that present differently in children, such

as intestinal failure–associated liver disease (IFALD). When the intestine is unable to absorb adequate nutrition, frequently due to neonatal short bowel syndrome,^[14] parenteral nutrition is a lifesaving intervention. However, 20%–30% of children receiving prolonged parenteral nutrition will develop IFALD.^[15] Pediatric IFALD is characterized by cholestasis and fibrogenesis while in adults steatohepatitis is seen more commonly.^[16] Liver injury seen in IFALD, such as cholestasis, inflammation, and fibrosis, can lead to end-stage liver disease.^[17] The pathogenesis of IFALD is multifactorial, not fully elucidated and is a result of intrinsic and extrinsic factors. More specifically, the intestinal microbiome and components found in parenteral nutrition are expected to play a role in IFALD, with the activation of hepatic macrophages.^[18]

In both the fetal and adult liver, single-cell RNA sequencing (scRNA-seq) has been instrumental in gaining an in-depth understanding of the liver's cellular heterogeneity and complexity. Based on the relative wealth of adult scRNA-seq data, we can now compare adult to pediatric liver and establish commonalities and pediatric-specific differences. A map of the healthy pediatric liver will also enable a better understanding of childhood liver diseases, such as IFALD. Here, we analyzed healthy human pediatric liver tissue and have made a pediatric liver single-cell map as a community resource. Using this map as a comparator, we present the first scRNA-seq map of the normal pediatric liver

and the pediatric IFALD liver and identify disease-associated differences in cell states.

METHODS

Liver sample collection

Healthy human liver tissue from the caudate lobe (and in 3 cases, right lobes) was obtained from neurologically deceased donor livers acceptable for liver transplantation and without evidence of histopathological liver disease, some of which have been previously published (Supplemental Table S1, <http://links.lww.com/HC9/C130>). IFALD samples were from children with IFALD undergoing an elective surgery due to their short bowel syndrome, and the samples are core-needle biopsies. Healthy adult samples were collected with institutional ethics approval from the University Health Network (REB# 14-7425-AE) and healthy and diseased pediatric samples through the Hospital for Sick Children (REB# 1000064039). All research was conducted in accordance with the Declarations of Helsinki and Istanbul, and written informed consent was obtained from living participants or, for pediatric or deceased donors, from their legal guardians or representatives. Samples were collected and processed for scRNA-seq, as described.^[19,20]

Single-cell RNA-seq data analyses

Full details are in the Supplemental Material, <http://links.lww.com/HC9/C130>, but in brief, sequencing reads were aligned using 10x Genomics Cell Ranger 3.1.0 software to the reference human transcriptome (GRCh38-Ensembl 93; Cell Ranger reference package-3.0.0). The resulting counts were processed using Seurat,^[21–24] SoupX,^[25] *rPCA*,^[26,27] cell cycle scoring,^[28] and SCINA.^[29] For cell type annotation, cells were clustered using the Seurat functions FindNeighbors and FindClusters (30 principal components and a resolution of 0.5). Then clusters were assigned a cell type label based on SCINA using broad cell type markers and then confirmed and/or refined with subclustering and manual annotation (Supplemental Table S2, <http://links.lww.com/HC9/C130>). Clusters of cells expressing multiple markers (often immune cells expressing LSEC markers) were annotated as doublets, except for cells expressing both myeloid and erythrocyte markers, which were labeled “Myeloid Erythrocytes (phagocytosis).” Differential expression of individual genes between healthy pediatric and adult or IFALD samples was tested in each cell type, using the *FindMarkers* function in Seurat^[30] on log-normalized counts. To explore the pathways related to differential expression with age and IFALD, we examined the enrichment of

gene ontology groups fgsea.^[31] Cell-cell interactions were inferred using CellPhoneDB.^[32] Comparison to fetal liver^[2] was done using varimax rotations of the principal components after integration.^[33]

Spatial transcriptomics

From 5 livers, 7 formalin-fixed paraffin-embedded liver sections (1 liver sampled 3 times) were applied to Xenium slides following the manufacturer's recommended protocols (10x Genomics) (Supplemental Table S3, <http://links.lww.com/HC9/C130>). Then they were run on the Xenium Analyzer at the Princess Margaret Genome Centre using the Human Multi-Tissue plus 100 liver-specific custom markers (Supplemental Table S4, <http://links.lww.com/HC9/C130>). For all spatial data, sections used were deemed normal by a pathologist's evaluation of hematoxylin and eosin stain. One sample (C94_2) contained a bile duct hamartoma and was excluded from analysis. Transcript counts and coordinates were exported from Space Ranger (10x Genomics). Further details on segmentation using BICell,^[34] cell type annotation, and zonation of hepatocytes are in the Supplemental Materials, <http://links.lww.com/HC9/C130>.

Myeloid intracellular cytokine and immunofluorescent staining

The IL-1 β secretion response by cells was assessed through flow cytometry by stimulating biobanked total liver homogenate cell suspension specimens with lipopolysaccharide (LPS). The gating strategy for both cell surface markers and intracellular markers was based on Fluorescence Minus One controls for each marker. Live CD45⁺CD3⁺CD68⁺CD14⁺ were targeted. The intracellular cytokine IL-1 β gating strategy was based on the fluorescence seen in both Fluorescence Minus One and the unstimulated control. Events were acquired using the Sony ID7000 spectral analyzer (6-laser 320–637 nm). Paraffin-embedded sections from healthy pediatric and IFALD liver were stained and quantified as described.^[35] Details are provided in the Supplemental Materials and antibodies are listed in Supplemental Table S5, <http://links.lww.com/HC9/C130>.

Data availability

The healthy pediatric liver map and IFALD data are available through CELLxGENE: <https://cellxgene.cziscience.com/collections/ff69f0ee-fef6-4895-9f48-6c64a68c8289>. Spatial transcriptomics data are available for exploration through a Shiny application:

macparlandlab.shinyapps.io/pediatric_liver_spatial. Spatial transcriptomics data are available under: GSE286254, and associated hematoxylin and eosin images are available at: zenodo.org/records/15691785. The single-cell map is on the Human Cell Atlas Data Portal: <https://explore.data.human-cellatlas.org/projects/febdadd-ad3c-4f4a-820f-ade15c48545a>.

In the interest of patient privacy, pediatric ages are published as a range. Exact age can be provided upon reasonable request. All code for analysis presented here is available at github.com/redgar598/liver_ped_map. Artificial intelligence tools were used to improve the readability and language of this work with the authors' oversight and careful review.

RESULTS

Landscape of pediatric liver cells

We generated 54,629 high-quality single-cell liver transcriptomes from 9 pediatric neurologically deceased liver donors (referred to as "healthy") and 3

IFALD donors (Table 1 and Supplemental Table S1, <http://links.lww.com/HC9/C130>). For comparison, we have used 26,372 liver cells from 7 healthy adult patients (Table 1 and Supplemental Table S1, <http://links.lww.com/HC9/C130>). Single-cell profiles were partitioned into 35 clusters, which we annotated using known markers (Figures 1A–C, Supplemental Table S2, <http://links.lww.com/HC9/C130>). All coarse clusters are well represented across technical variables and generally proportional across individuals (Supplemental Figures S1 and S2, <http://links.lww.com/HC9/C130>; entropy > 0.48). While distinct parenchymal and non-parenchymal compartments are seen, *ALB* expression was also seen in *PTPRC*+ cells, suggesting ambient mRNA contamination from hepatocytes in all other cells (Figure 1D). Ambient mRNA was seen to a greater extent in adult samples (Supplemental Table S1, <http://links.lww.com/HC9/C130>), but we expect this is a chance technical effect and not an age-related biological effect. All coarse cell types identified in the healthy pediatric map are also seen in adults (except for a population of neutrophils, 70% of which were from 1 adult sample, ID: C97) (Figures 1E, F, Supplemental Figure S3, <http://links.lww.com/HC9/C130>).

TABLE 1 Demographics of patients

Condition	Individual	Age (y)	Tissue	Sex
Healthy pediatric	C104	1–4	Biopsy	M
	C105	5–14	Caudate	F
	C85	5–14	Caudate	M
	C115	5–14	Caudate	M
	C93	5–14	Caudate	F
	C102	15–19	Right lobe	F
	C113	15–19	Right lobe	M
	C64	15–19	Caudate	M
	C96	15–19	Caudate	F
IFALD pediatric	IFALD006 <i>Mild IFALD</i>	5–14	Biopsy	M
	IFALD030 <i>Progressive IFALD</i>	0–11 mo	Biopsy	F
	IFALD073 <i>Mild IFALD</i>	0–11 mo	Biopsy	F
			PBMC	
Healthy adult	C82	26	Caudate	M
	C70	48	Caudate	F
	C97	57	Caudate	F
	C68	61	Caudate	F
	C39	65	Caudate (NPC)	M
			Caudate (TLH)	
	C54	67	Caudate	F
	C88	69	Caudate	F

Abbreviations: NPC, nonparenchymal cells; PBMC, peripheral blood mononuclear cells; TLH, total liver homogenate.

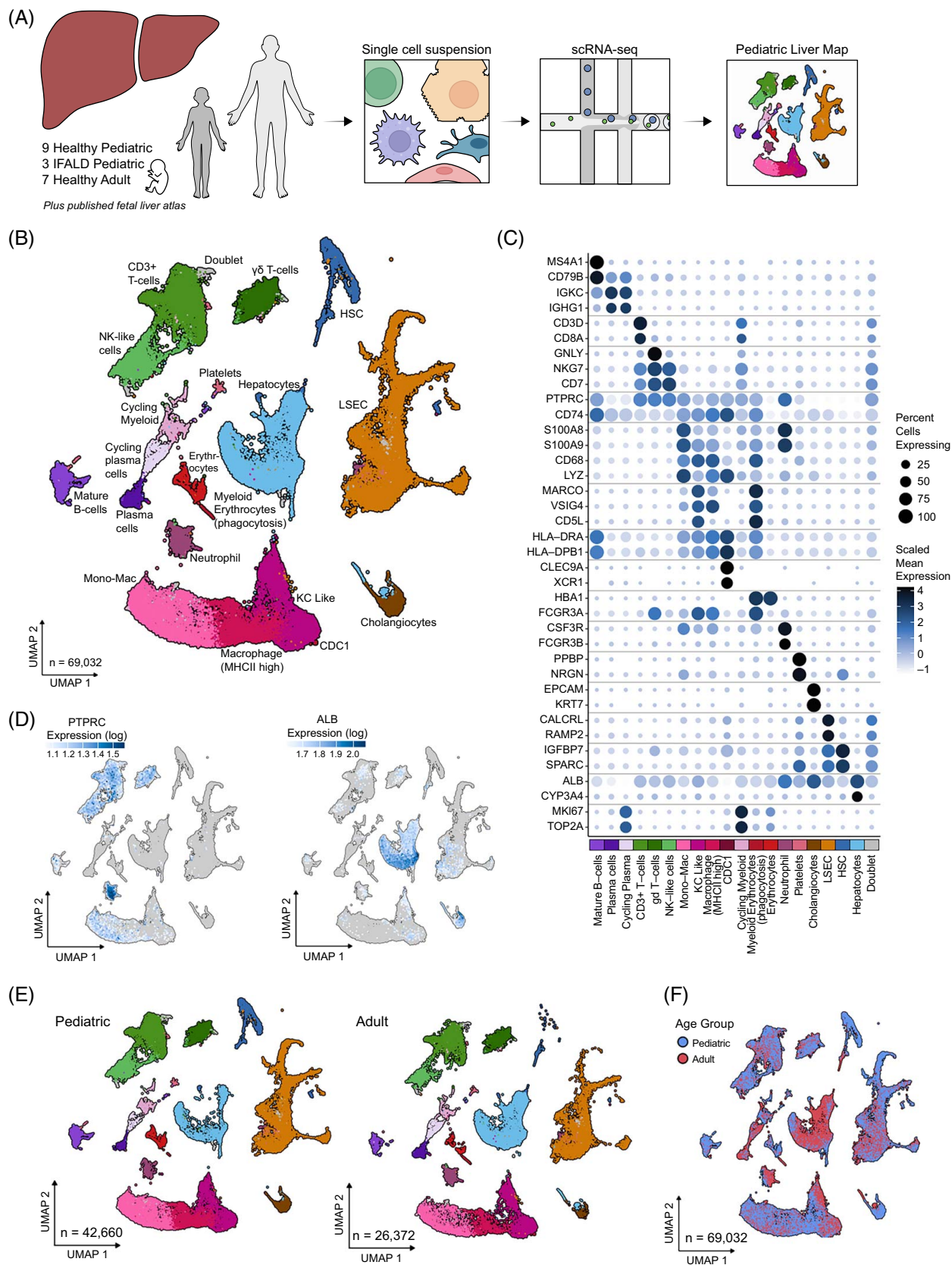


FIGURE 1 Landscape of cells in the pediatric liver shows similar coarse clusters to the adult liver. (A) Overview of the map generation process. (B) UMAP of combined healthy pediatric and adult liver cells. (C) Gene expression of key markers used for cell type annotation. The color of the points represents the gene expression level, and the size represents the percentage of cells of a type expressing the gene at all. (D) Pediatric liver map colored by expression of a key hepatocyte marker (ALB) and a nonparenchymal cell marker (PTPRC: ie, CD45). (E) The pediatric liver map split by age group. (F) The pediatric liver map colored by age group.

Immune activity of pediatric and adult liver resident myeloid cells

In both adult and pediatric livers, myeloid cells selected based on marker genes (Supplemental Table S2, <http://links.lww.com/HC9/C130>) could be subclustered into 3 major populations: KC-like liver resident macrophages (*VSIG4*, *MARCO*, and *CD5L*), recently recruited monocyte-like (Mono-Mac) myeloid cells (*S100A8/9* and *LYZ*), or major histocompatibility class II (MHCII) high myeloid cells (*HLA-DRA/DPB1/DQB1*) (Figures 1B, 2A). A minor population of MHCII and *CLEC9A* high cells was seen in both pediatric and adult livers. These may be conventional type 1 dendritic cells (cDC1),^[36] but as there were only 38 of these cells in the healthy pediatric and adult samples, little can be concluded from this population.

When comparing pediatric to adult in each of the 3 major myeloid populations, genes associated with immune activation were more highly expressed in pediatric livers. In KC-like cells in particular, key chemokines (*CCL3* and *CCL4*) were more highly expressed as well as *IL1B* (Figure 2B and Supplemental Table S6, <http://links.lww.com/HC9/C130>). The differential expression results were confirmed to be robust to technical confounding of assay chemistry, by repeating the analysis using only 3' samples (Supplemental Table S1, <http://links.lww.com/HC9/C130> and Supplemental Figure S4, <http://links.lww.com/HC9/C130>). The immune activation gene signature seen in pediatric KC-like cells has previously been seen in fetal liver macrophages.^[2,37] The combined fetal and pediatric liver data show even higher immune activation in the fetal liver (Supplemental Figure S5, further detail in Supplemental Materials, <http://links.lww.com/HC9/C130>), suggesting that the KC-like immune activation may be highest in fetal liver and wane through gestation and aging. These genes and others contributed to a significant enrichment of the "IL-18 signaling" pathway in genes more highly expressed in pediatric KC-like cells (Figure 2B and Supplemental Figure S6, <http://links.lww.com/HC9/C130>). In the MHCII high myeloid cells, *HMOX1* and *APOE* are more highly expressed in pediatric cells and drive an enrichment of the pathway "regulation of epithelial cell proliferation" (Figure 2B and Supplemental Figure S6, <http://links.lww.com/HC9/C130>; Supplemental Table S7, <http://links.lww.com/HC9/C130>). In Mono-Mac cells from pediatric samples, cellular stress pathways were enriched, including elevated expression of *AREG* and several heat shock protein-related genes (Figure 2B and Supplemental Figure S6, <http://links.lww.com/HC9/C130>; Supplemental Table S8, <http://links.lww.com/HC9/C130>).

Focusing on the KC-like cell immune activation, we observed that pediatric KC-like cells are predicted to interact with other myeloid cells and T cells through known ligand-receptor pairs. Specifically, *CCL3* and *CCL4* expressed in KC-like cells could be interacting

with Mono-Mac and MHCII high myeloid cells (through *CCR1*) and T-cell populations (through *CCR5* and *CCR1*) (Figure 2C), suggesting KC in the pediatric liver could be recruiting T cells and promoting monocyte chemotaxis. Looking at interactions inferred from expression of known IL-1 β binding partners, interactions were predicted between KC-like cells and many other cell types: hepatocytes, cholangiocytes, neutrophils, Mono-Mac cells, and MHCII high myeloid cells (Figure 2C). However, there were also predicted interactions between IL-1 β and the IL-1 β receptor inhibitor in neutrophils, Mono-Mac cells, and MHCII high myeloid cells, but not in hepatocytes and cholangiocytes (Supplemental Figure S7, <http://links.lww.com/HC9/C130>). Therefore, potentially, the interaction of IL-1 β with its receptor is inhibited in myeloid cells but not in hepatocytes and cholangiocytes, allowing activated pediatric KC-like cells to signal to parenchymal and epithelial cells specifically.

From these data, we asked the question of whether the higher expression of immune-related genes could be linked to protein-level functional differences related to cytokine and chemokine secretion. Having seen *IL1B* more highly expressed in the pediatric liver, we tested the capacity of myeloid cells (CD68⁺CD14⁺) isolated from pediatric and adult livers to secrete IL-1 β upon LPS stimulation (Supplemental Figure S8, <http://links.lww.com/HC9/C130>). We found a significantly higher frequency of pediatric myeloid cells secreting IL-1 β in response to LPS compared with adult myeloid cells ($p < 0.05$; Figures 2D, E). This confirms that the immune activation signature seen in the pediatric scRNA-seq map does confer a higher inflammatory potential compared with the adult liver.

Zonation of immune cells within the liver is a dynamic system. We therefore examined the zonation of gene expression in myeloid cells to understand if spatial dynamics in liver transcriptomics could explain some differences seen between the pediatric and adult liver. We explored the zonation of a panel of 477 genes using the Xenium spatial transcriptomics platform in 2 pediatric and 3 adult livers (Supplemental Table S2, <http://links.lww.com/HC9/C130>; Figures 3A–C, Supplemental Figure S9, <http://links.lww.com/HC9/C130>). Of the 70 genes significantly differentially expressed in pediatric KC-like cells in the single-cell pediatric map, 10 genes were included in the spatial panel. Of these, 8 genes were zoned (false discovery rate < 0.001) in KC-like cells (Supplemental Table S9, <http://links.lww.com/HC9/C130>, Figures 3D–F), which have more zoned genes than expected by chance ($p < 0.05$). This included KC marker genes (*MARCO* and *CD5L*), which were zoned within KC-like cells in all samples (Figure 3F). The zonation of the KC marker genes suggests that the observed differential gene expression in the dissociated map could be the result of underlying shifts in KC zonation in the pediatric liver.

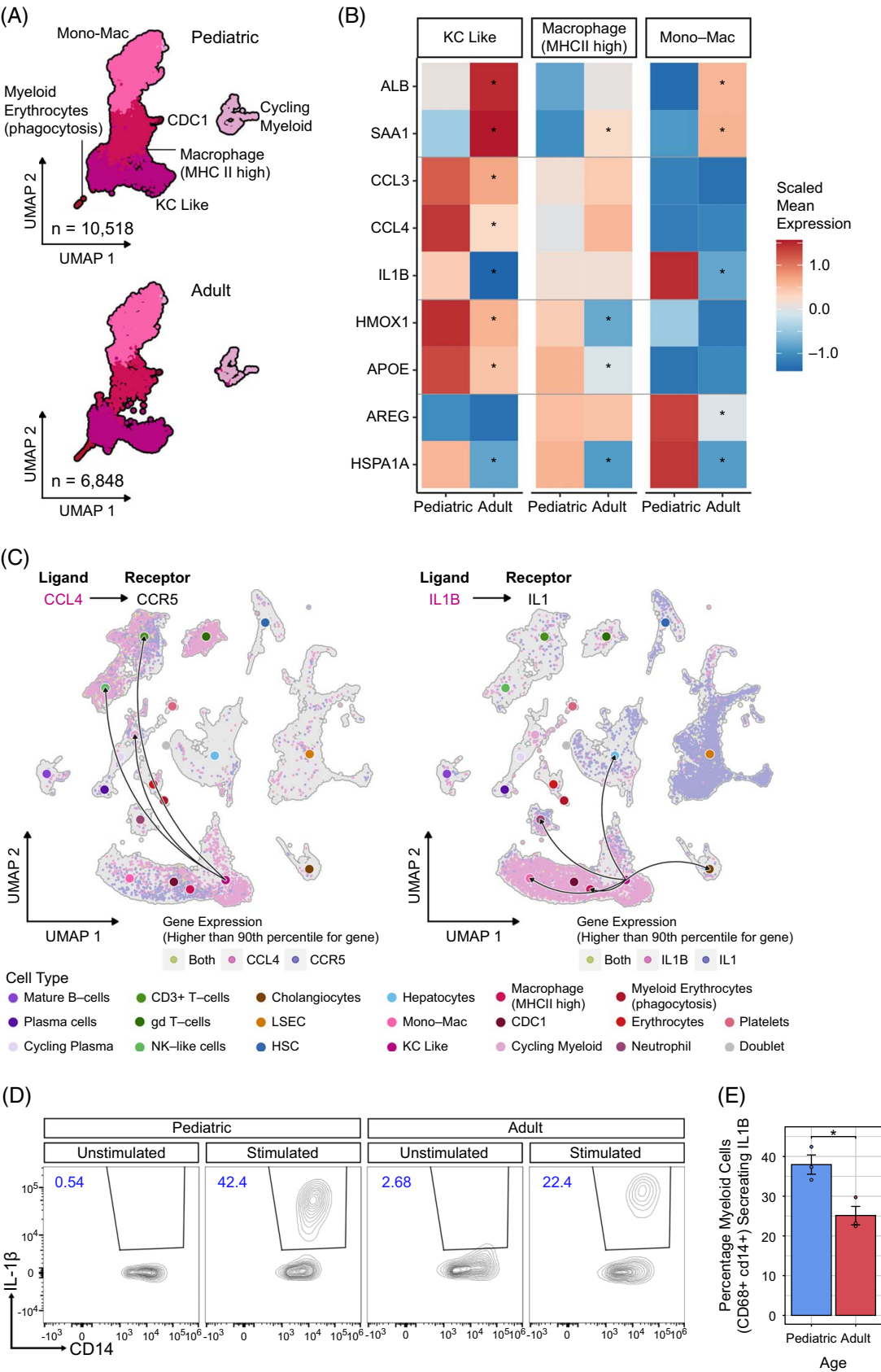


FIGURE 2 Pediatric liver myeloid cells express more inflammatory cytokines than adult cells. (A) UMAPs of liver myeloid cells split by sample age group. (B) Differentially expressed genes in each myeloid cell type. Rows show individual genes, and columns show samples split by age group. Horizontal lines divide genes into the following categories: higher expression in adults in all myeloid types, higher expression in pediatric

KC-like cells, higher expression in pediatric MHCII high cells, and higher expression in pediatric Mono-Mac cells. (C) Predicted cell-cell interactions between KC-like cells and all other cell types. Individual cells in the UMAP are colored by the expression of the ligand and/or receptor. Left panel: CCL4-CCR5, right panel: IL1B-IL1. Arrows on the connecting curves point from ligand to receptor, and curves are only shown for significant cell-cell interactions. Larger points that curves connect are colored to indicate the cell population. (D) Percentage of IL-1 β + secreting myeloid cells (CD68+CD14+) in the unstimulated control and LPS-stimulated conditions of pediatric and adult myeloid cells. (E) Stimulated adult versus pediatric cells with the percentage of myeloid cells (CD68+CD14+) secreting IL-1 β is shown. Abbreviation: LPS, lipopolysaccharide. *Bonferroni-adjusted p-value < 0.005.

Of note, 1 sample from C94 (C94_2) captured a bile duct hamartoma (Supplemental Figure S10, <http://links.lww.com/HC9/C130>). This sample was excluded from analyses but the data will be released along with the other spatial data presented here as it may be of interest to the community.

Fibrosis and immune activity in IFALD liver

Having established the healthy pediatric map, we then applied this map as a comparator to explore the cellular complexity of liver biopsies from pediatric IFALD patients (Figure 4A). In the combined adult, healthy pediatric and IFALD map, we observed 2 distinct populations of HSCs (Figure 4B). HSC population 1 is made up of mainly healthy pediatric HSCs (92% of cells), and HSC population 2 is made up of mainly IFALD (48% of cells) and adult HSCs (23% of cells), suggesting HSCs in IFALD are more similar to healthy adult than healthy pediatric HSCs. Comparing these 2 HSC populations, we saw fibrosis genes (*PDGFRA*, *CXCL12*, *COL1A1*, and *IGFBP3*) more highly expressed in HSC population 2, which is mainly adult and IFALD cells (Figure 4C; Supplemental Table S10, <http://links.lww.com/HC9/C130>). Fibrosis is a key feature of IFALD, and it is interesting to confirm HSC activation at the single-cell level. Without the healthy pediatric map, IFALD HSCs would have only been compared with healthy adults, and this evidence of fibrosis at the single-cell level may have been missed, as several fibrosis markers (*PDGFRA*, *CXCL12*, and *IGFBP3*) were not differentially expressed when comparing IFALD to adult HSCs (Supplemental Table S11, <http://links.lww.com/HC9/C130>).

Since the patients with IFALD are younger than the healthy pediatric individuals, we performed differential expression analysis in HSCs using the most closely age-matched individuals. We compared healthy pediatric HSCs from one individual in the 1–4-year age range to HSCs from 2 patients with IFALD in the 0–11-month age range. In this subset analysis, 64% of genes identified in the full cohort were also significant (false discovery rate < 0.005, absolute fold change > 1,) including key fibrosis markers discussed (Supplemental Figure S11, <http://links.lww.com/HC9/C130>).

The IFALD HSC findings highlight the limitations of using healthy adults as a pediatric disease comparator; an alternate approach used previously has employed

other pediatric liver diseases as comparators.^[38] Looking at cholangiocytes from a previously published biliary atresia map where the original comparator was cells from patients with choledochal cysts, we observed higher expression and pathway enrichment of MHCII and MHCII signaling in both biliary atresia and choledochal cysts compared with healthy pediatric liver (Supplemental Material; Supplemental Figures S12 and S13, <http://links.lww.com/HC9/C130>). As this signal is shared in cholangiocytes from patients with biliary atresia and choledochal cysts, it was not observed in the original publication.

Turning to immune populations, we saw several populations unique to IFALD and not seen in either healthy pediatric or adult populations. Specifically, we saw more pre-B cells (*IGLL1*+ but *MS4A1*-)^[39,40] in IFALD. We also identified plasmacytoid dendritic cells (pDCs; *IL3RA*+ and *PLAC8*+),^[2] which were more abundant in IFALD (Figures 4E–G). We were also interested in any macrophage-specific differences in IFALD. In terms of differences in cell type abundance, we see similar levels of major cell types (Figure 5A). We did see the cDC1 population more abundant in IFALD (Figure 5A), and cDCs have been seen previously to be more abundant in metabolic dysfunction–associated steatohepatitis (MASH).^[41] However, both the pDC and cDC1 differences could result from the differences in sample processing and the inclusion of more blood in the IFALD liver samples (Supplemental Material; Supplemental Figure S14, <http://links.lww.com/HC9/C130>).

When comparing healthy pediatric to IFALD in the 3 major myeloid populations, we saw potential shifts in cell identity and function. In Mono-Mac myeloid cells, we see *IL1B* more highly expressed in IFALD than in healthy pediatric (Figure 5B and Supplemental Table S12, <http://links.lww.com/HC9/C130>), suggesting a similar immune activation seen when comparing pediatric to adult. In addition, we observed a potential profibrotic state of IFALD myeloid cells. In KC-like cells, we saw higher expression of profibrotic genes (ie, *LY96*) (Figure 5B and Supplemental Table S13, <http://links.lww.com/HC9/C130>). The overexpression of *LY96* is unique to IFALD and not seen in comparison to other pediatric liver diseases (Supplemental Material; Supplemental Figure S15, <http://links.lww.com/HC9/C130>). As the protein product of *LY96* (MD-2) is a component of Toll-like receptor 4 (TLR4),^[42] we wanted to validate its increased abundance in IFALD myeloid cells at the protein level. Using immunofluorescence staining of

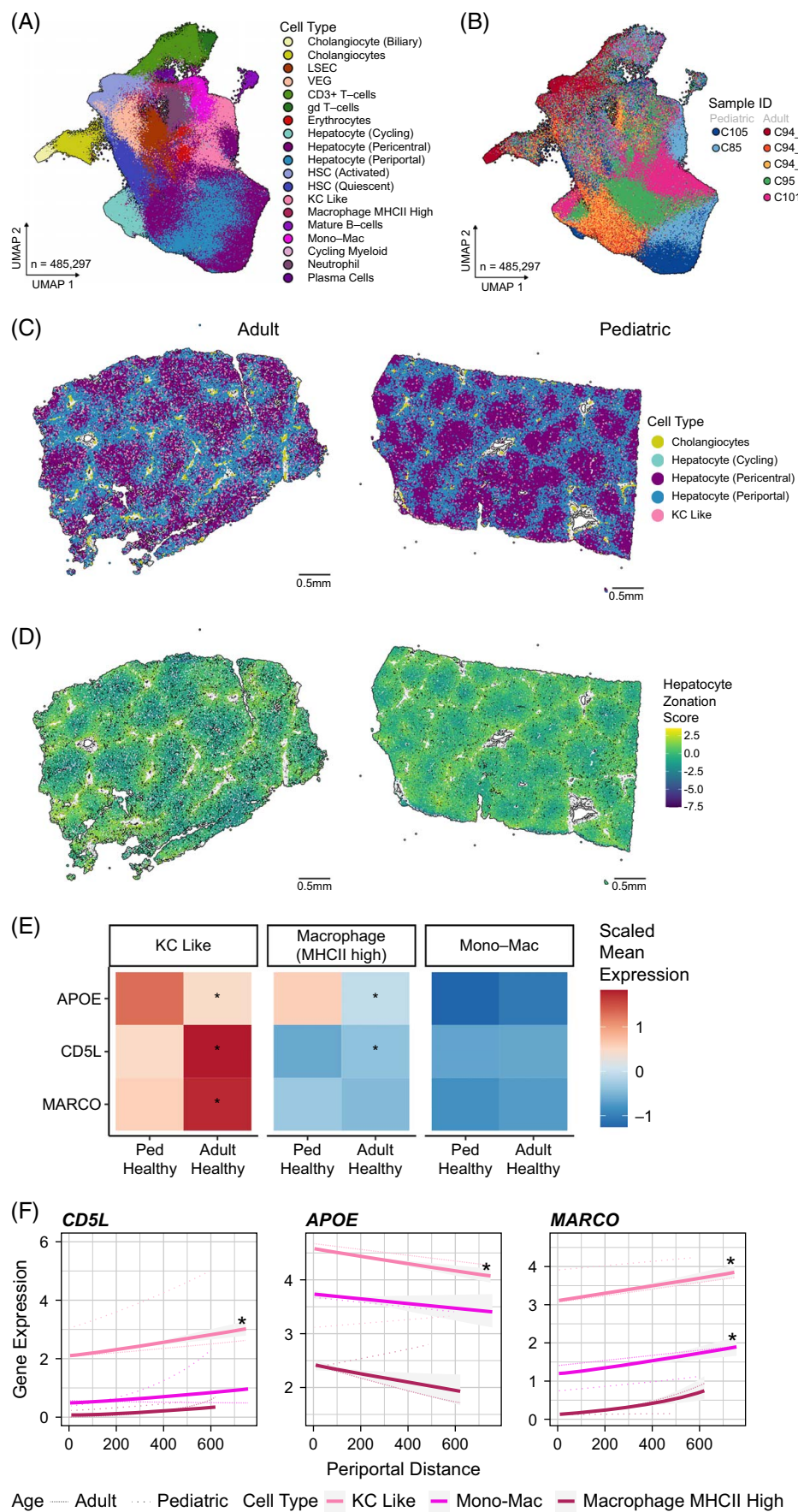


FIGURE 3 Zonation is successfully captured in both pediatric and adult spatial transcriptomics at the single-cell level. UMAP of combined healthy pediatric and adult liver cells from the spatial transcriptomics assay, colored by (A) cell type and (B) donor ID. (C) Representative adult (C94_4) and pediatric (C105) spatial transcriptomics samples with points representing cells colored by cell type and positioned in their physical location in the tissue. Only the listed cell types are shown to highlight the zonation between the portal and central veins. (D) Only hepatocytes are shown with cells colored by zonation score. (E) Differential expression, in the dissociated single-cell map, of genes present in the spatial data. (F) The same genes are significantly differentially expressed with inferred distance to a portal vein in KC-like cells in the spatial transcriptomics samples. Thicker lines represent the trend across samples, with thinner lines for the trend in pediatric and adult samples separately. *FDR < 0.001.

healthy pediatric and IFALD samples, we confirmed the higher proportion of MD-2⁺CD68⁺ myeloid cells in IFALD compared with healthy pediatric myeloid cells ($p < 0.05$; Figures 5C, D).

DISCUSSION

The pediatric liver represents an important but understudied window of development. Using single-cell transcriptome profiling, we describe the cellular micro-environment of the pediatric liver in comparison to adults and pediatric liver disease. This map is a resource for the community to study pediatric liver disease. Inherent differences, like the immune activation in pediatric myeloid cells, mean the pediatric map will serve as an important comparator to account for normal differences with age in the liver and with disease conditions.

The function of macrophage immune activation during liver development is unclear, but a similar trend has been seen in other age ranges and tissues

In fetal tissues, including the liver, there is greater macrophage immune activation at earlier gestational ages.^[37] A possible function for the immune activation is suggested by the higher expression of genes related to epithelial cell proliferation in MHCII myeloid cells (*HMOX1* and *APOE*) and the potential for myeloid cells to signal cholangiocytes and hepatocytes through *IL1B*. Shifts in liver immune composition have been seen to be a crucial element in healthy liver development.^[43] The observed immune activation of KC-like cells could be a normal part of the growth and structural development of parenchymal and epithelial cells in the pediatric liver, a process that is later suppressed in adulthood, once the liver is fully formed.

Characterizing the pediatric liver could have important clinical implications

Age-related differences in the chemokines we have seen in the liver are also seen in pediatric blood compared with adult blood.^[44] There is an observed decline with age in the abundance of the proteins CCL4,

IL-1 β , and CXCL8 over a similar age range as our samples, but no association between CCL3 and age was seen.^[44] In a separate cohort, CCL4 and CXCL8 abundance in the blood also declined with age, but again, CCL3 was not significant.^[45] Potentially, the immune activation we have seen in the pediatric liver is involved in shaping the liver's growth and structure, and the age-related differences in these secreted chemokines can be seen in the blood.

The differences we have found between pediatric and adult livers illustrate the value of an age-matched comparator for studying pediatric liver disease

The signal (*COL1A1*⁺, *PDGFRA*⁺, *CXCL12*⁺, and *IGFBP3*⁺) of fibrosis in IFALD-enriched HSCs was expected, given that IFALD is known to involve liver fibrosis. However, if IFALD HSCs had only been compared with adult HSCs, then this fibrosis would likely have been missed. This highlights the importance of using age-appropriate controls when studying pediatric diseases, as comparisons to adult tissues may mask disease-specific changes in young patients. Fibrosis, observed at the single-cell level in IFALD, is an important observation as it is similar to the signal seen in MASH and may suggest some pathogenic similarities between the 2 diseases,^[46] but is distinct from differences seen in single-cell transcriptomics of primary sclerosing cholangitis.^[8] As metabolic dysfunction-associated fatty liver disease, MASH, and primary sclerosing cholangitis all present uniquely in children compared with adults, the finding of immune activation in the pediatric liver may explain some of the clinically observed differences, as the pediatric liver is generally a more immune-active background for the disease.^[47,48] These differences in immune activation may also explain the different histology findings in IFALD between children and adults with the disease. In addition to the fibrosis signature seen in HSCs, differences in myeloid subpopulations would likely also have been missed if pediatric IFALD were only compared with healthy adults. We saw *IL1B* more highly expressed in IFALD Mono-Mac cells, suggesting an IL-18 signaling role in IFALD in Mono-Mac cells. We did not see the same higher expression of *IL1B* in IFALD KC-like cells compared with healthy pediatric livers, but *IL1B* in IFALD KC-like cells was different from that in adult KC-

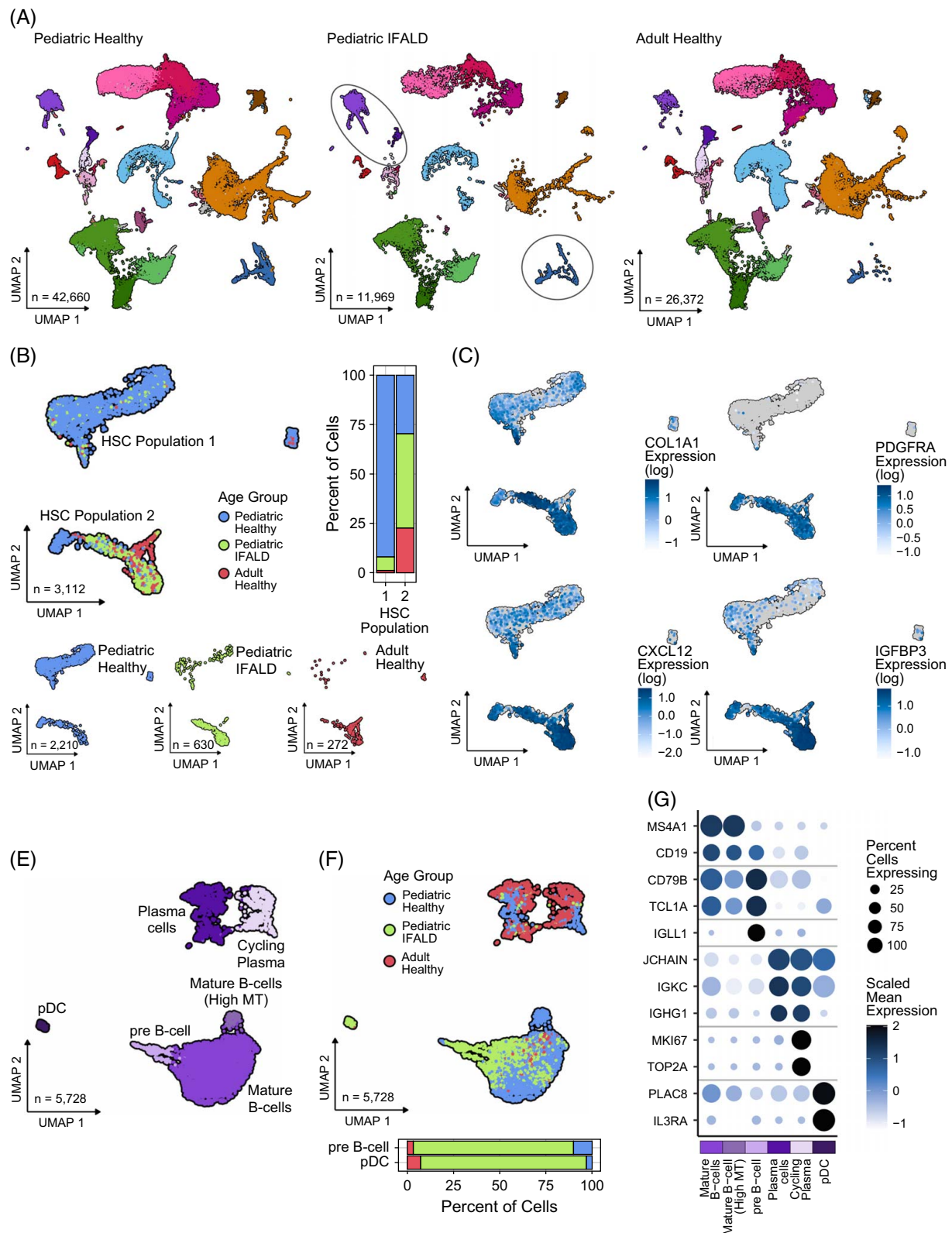


FIGURE 4 IFALD HSCs are more fibrotic than nondiseased livers and contain unique B-cell types. (A) UMAP of liver cells with key cell types highlighted, where differences in IFALD are described. (B) HSC UMAP colored as well as split by age and disease status, with a barplot showing the composition of each HSC population. (C) UMAPs colored by differentially expressed fibrosis genes. UMAP of B cells colored by (E) cell type or (F) sample age and disease group, with a barplot showing the composition of pre-B cells and pDCs. (G) Gene expression of key B-cell markers used for B-cell annotation. The color of the points represents the gene expression level, and the size represents the percentage of cells of a type expressing the gene at all. Abbreviation: IFALD, intestinal failure–associated liver disease.

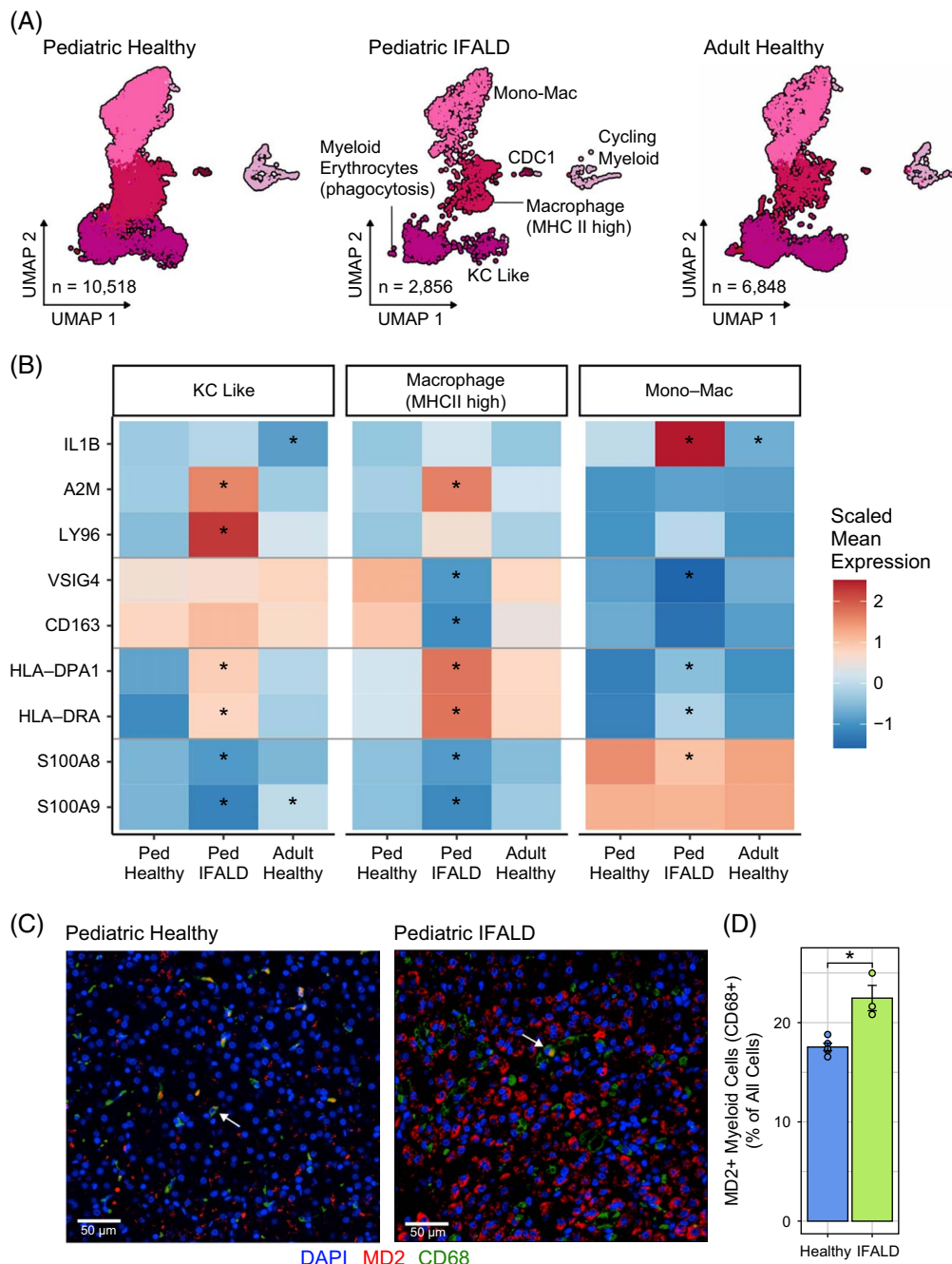


FIGURE 5 IFALD myeloid cells more highly express profibrotic genes than nondiseased livers. (A) UMAP of liver myeloid cells split by age and disease. (B) Differentially expressed genes for each myeloid cell type. Rows show individual genes, and columns show samples split by age and disease. The horizontal lines divide genes into the following categories: higher expression in IFALD in KC cells, lower expression in IFALD MHCII high cells, higher expression in IFALD MHCII high cells, and lower expression in IFALD KC-like and MHCII high cells. *Bonferroni-adjusted p-value < 0.005. (C) Representative IF images of pediatric healthy and IFALD livers. (D) Quantification of the MD2+CD68+ cells. Abbreviation: IAFLD, intestinal failure–associated liver disease.

like cells, likely due to the generally higher immune activation of the pediatric liver. Our findings support previous publications showing the major role of IL-1 β in the pathogenesis of IFALD through downregulation of LXR and canalicular ABCG5/G8.^[15] As with HSCs, if we had only compared IFALD to healthy adults, the immune-activated state of the pediatric KC-like population may have been incorrectly attributed to IFALD.

With this age-matched comparator, we were able to observe a potential role of myeloid cells in contributing to IFALD fibrosis

We have seen lower expression of *S100A8* and *S100A9* in IFALD myeloid cells, and this is similarly seen in metabolic dysfunction–associated fatty liver

disease myeloid cells,^[49] as well as a similar profibrotic (ie, LY96+) role of IFALD KC-like cells is also seen in MASH.^[46] One potential mechanism in the pathogenesis of IFALD is the crossing of LPS from the gut into the portal system due to leaky gut, typical of children with short bowel syndrome.^[18] The protein encoded by LY96, MD-2, is a component of TLR4, the core receptor for LPS. The LY96+ KC-like population in IFALD may support the theory that inflammation and eventual failure of the liver, in part, occur through LPS-driven inflammation at the portal veins. This is a promising finding as MD-2 is a druggable target with inhibitors being developed for the treatment of systemic sclerosis.^[50]

The healthy pediatric and IFALD maps will be improved with the continual integration of more samples

Some technical confounders cannot be fully controlled for in the current analysis. For example, the adult samples used for comparison had higher levels of ambient mRNA contamination than the pediatric samples. In addition, the IFALD samples were derived from liver biopsies, whereas the healthy pediatric map was generated from perfused caudate lobes of neurologically deceased donors. These can be overcome with the future inclusion of more diverse samples, integrated across labs. Another confounder between pediatric IFALD and the healthy pediatric samples, which may explain some of the cell populations unique to IFALD, is a difference in age. Two of the 3 IFALD sample donors were under 1 year of age, and the youngest healthy donor was a 2-year-old patient. As the liver is a site of hematopoiesis during gestation, the abundance of pre-B cells in IFALD may be a normal feature of livers under 1 year of age and not a unique feature of IFALD. This is supported by the observation of a similar population (by gene expression signature) of pre-B cells in the fetal liver.^[37] As pediatric liver samples are exceedingly rare, it is important to share this map even with the current caveats. This resource has enabled key insight into pediatric liver disease and will be a valuable resource to the community.

AUTHOR CONTRIBUTIONS

Conceptualization: Rachel D. Edgar, Yaron Avitzur, Gary D. Bader, Sonya A. MacParland. Formal analysis: Rachel D. Edgar, Diana Nakib, Sai Chung, Patricia Lumanto, and Cornelia Thoeni. Investigation: Rachel D. Edgar, Diana Nakib, Damra Camat, Sai Chung, Patricia Lumanto, Jawairia Atif, Catia T. Perciani, Xue-Zhong Ma, and Justin Manuel. Resources: Blayne Sayed, Koen Huysentruyt, Amanda Ricciuto, Ian McGilvray, Yaron Avitzur, Gary D. Bader, and Sonya A. MacParland. Funding acquisition: Ian McGilvray, Yaron Avitzur,

Gary D. Bader, and Sonya A. MacParland. Project administration: Nilosa Selvakumaran. Writing—original draft: Rachel D. Edgar. Writing—review and editing: all authors.

ACKNOWLEDGMENTS

This publication is part of the Human Cell Atlas— <https://www.humancellatlas.org/publications>. The authors acknowledge the Princess Margaret Genomics Centre, the Pathology Research Program, and the Advanced Optical Microscopy Facility at University Health Network for their support and services. The graphical abstract was created with Biorender.com. The authors acknowledge Dr Michael Cheng and Dr Harry Sutton for their comments and insights on the study. The authors acknowledge Dr Stacey Huppert for informal peer review of this manuscript.

FUNDING INFORMATION

Rachel D. Edgar is funded by a postdoctoral fellowship from the Canadian Network on Hepatitis C (CanHepC). CanHepC is funded by a joint initiative of the Canadian Institutes of Health Research (CIHR) (NHC-142832) and the Public Health Agency of Canada (PHAC), as well as by a CIHR fellowship (FRN-201015) and an Ajmera Transplant Research Fellowship. Diana Nakib has received doctoral and postdoctoral funding from CIHR (CGS-D and CAN TAP Talent Clinical Research Training Fellowship). Damra Camat is funded by an NSERC CREATE CEAPRO graduate fellowship. This research is also funded by grant numbers CZF2019-002429, CZF2021-237921, and CZF2022-316558 from the Chan Zuckerberg Initiative DAF, an advised fund of Silicon Valley and from CIHR grant HIT168002 (Sonya A. MacParland, Gary D. Bader, Ian McGilvray, and Amanda Ricciuto). Funds were also provided by the University of Toronto's Medicine by Design, the Canada First Research Excellence Fund, Toronto General and Western Hospital Foundation, and the UHN Foundation.

CONFLICTS OF INTEREST

Gary D. Bader advises and owns stock in Adela Bio. He advises BioRender. The remaining authors have no conflicts to report.


ORCID

Rachel D. Edgar  <https://orcid.org/0000-0001-5507-6078>

Diana Nakib  <https://orcid.org/0000-0002-4046-2109>

Damra Camat  <https://orcid.org/0000-0001-8435-4073>

Sai Chung  <https://orcid.org/0000-0003-2684-7122>

Patricia Lumanto  <https://orcid.org/0009-0002-1155-9793>

Jawairia Atif  <https://orcid.org/0000-0001-6924-7376>

Catia T. Perciani  <https://orcid.org/0000-0003-0377-1778>
 Cornelia Thoeni  <https://orcid.org/0009-0004-8181-319X>
 Nilosa Selvakumaran  <https://orcid.org/0009-0006-4894-7297>
 Blayne Sayed  <https://orcid.org/0000-0003-3224-8871>
 Koen Huysentruyt  <https://orcid.org/0000-0002-6402-1762>
 Amanda Ricciuto  <https://orcid.org/0000-0001-9538-3005>
 Ian McGilvray  <https://orcid.org/0000-0003-4649-546X>
 Yaron Avitzur  <https://orcid.org/0000-0002-8072-5727>
 Gary D. Bader  <https://orcid.org/0000-0003-0185-8861>
 Sonya A. MacParland  <https://orcid.org/0000-0002-8036-1425>

REFERENCES

- MacParland SA, Liu JC, Ma X-Z, Innes BT, Bartczak AM, Gage BK, et al. Single cell RNA sequencing of human liver reveals distinct intrahepatic macrophage populations. *Nat Commun*. 2018;9:4383.
- Popescu D-M, Botting RA, Stephenson E, Green K, Webb S, Jardine L, et al. Decoding human fetal liver haematopoiesis. *Nature*. 2019;574:365–71.
- Guilliams M, Bonnardei J, Haest B, Vanderborght B, Wagner C, Remmerie A, et al. Spatial proteogenomics reveals distinct and evolutionarily conserved hepatic macrophage niches. *Cell*. 2022;185:379–396.e38.
- Fred RG, Steen Pedersen J, Thompson JJ, Lee J, Timshel PN, Stender S, et al. Single-cell transcriptome and cell type-specific molecular pathways of human non-alcoholic steatohepatitis. *Sci Rep*. 2022;12:13484.
- Zhao J, Zhang S, Liu Y, He X, Qu M, Xu G, et al. Single-cell RNA sequencing reveals the heterogeneity of liver-resident immune cells in human. *Cell Discov*. 2020;6:22.
- Ramachandran P, Dobie R, Wilson-Kanamori JR, Dora EF, Henderson BEP, Luu NT, et al. Resolving the fibrotic niche of human liver cirrhosis at single-cell level. *Nature*. 2019;575:512–8.
- Wesley BT, Ross ADB, Muraro D, Miao Z, Saxton S, Tomaz RA, et al. Single-cell atlas of human liver development reveals pathways directing hepatic cell fates. *Nat Cell Biol*. September 15 2022;24:1487–98.
- Andrews TS, Nakib D, Perciani CT, Ma XZ, Liu L, Winter E, et al. Single-cell, single-nucleus, and spatial transcriptomics characterization of the immunological landscape in the healthy and PSC human liver. *J Hepatol*. 2024;80:730–43.
- Taylor SA, Chen S-Y, Gadhvi G, Feng L, Gromer KD, Abdala-Valencia H, et al. Transcriptional profiling of pediatric cholestatic livers identifies three distinct macrophage populations. *PLoS One*. 2021;16:e0244743.
- Peters AL, DePasquale EAK, Begum G, Roskin KM, Woodle ES, Hildeman DA. Single-cell transcriptional landscape of liver transplant rejection reveals tissue persistence of clonally expanded, treatment-resistant T cells. *Am J Transplant*. August 12, 2025.
- Ginsberg G, Hattis D, Sonawane B. Evaluation of child/adult pharmacokinetic differences from a database derived from the therapeutic drug literature. *Toxicol Sci*. 2002;66:185–200.
- Blanco JG, Harrison PL, Evans WE, Relling MV. Human cytochrome P450 maximal activities in pediatric versus adult liver. *Drug Metab Dispos*. 2000;28:379–82.
- England K, Thorne C, Pembrey L, Tovo P-A, Newell M-L. Age- and sex-related reference ranges of alanine aminotransferase levels in children: European paediatric HCV network. *J Pediatr Gastroenterol Nutr*. 2009;49:71–7.
- Duggan CP, Jaksic T. Pediatric intestinal failure. *N Engl J Med*. 2017;377:666–75.
- Khalaf RT, Sokol RJ. New insights into intestinal failure-associated liver disease in children. *Hepatology*. 2020;71:1486–98.
- Lee WS, Chew KS, Ng RT, Kasmi KE, Sokol RJ. Intestinal failure-associated liver disease (IFALD): Insights into pathogenesis and advances in management. *Hepatol Int*. 2020;14:305–16.
- Pironi L, Joly F, Forbes A, Colomb V, Lyszkowska M, Baxter J, et al. Long-term follow-up of patients on home parenteral nutrition in Europe: Implications for intestinal transplantation. *Gut*. 2011;60:17–25.
- El Kasmi KC, Anderson AL, Devereaux MW, Fillon SA, Harris KJ, Lovell MA, et al. Toll-like receptor 4-dependent Kupffer cell activation and liver injury in a novel mouse model of parenteral nutrition and intestinal injury. *Hepatology*. 2012;55:1518–28.
- Nakib D, Perciani C, McGilvray I, Macparland S. Human liver core-needle biopsy processing protocol. *protocols.io*. Published online November 2022. Accessed September 12, 2025. <https://dx.doi.org/10.17504/protocols.io.8epv5jzwj1b/v1>
- MacParland S, Ma X-Z, Manuel J, Liu J, Bader G, McGilvray I. Human liver caudate lobe dissociation for ScRNA-seq. *protocols.io*. Published online February 2018. Accessed September 12, 2025. <https://dx.doi.org/10.17504/protocols.io.m9sc96e>
- Hao Y, Hao S, Andersen-Nissen E, Mauck WM, Zheng S, Butler A, et al. Integrated analysis of multimodal single-cell data. *Cell*. 2021;184:3573–87.
- Stuart T, Butler A, Hoffman P, Hafemeister C, Papalexi E, Mauck WM, et al. Comprehensive integration of single-cell data. *Cell*. 2019;177:1888–1902.e21.
- Satija R, Farrell JA, Gennert D, Schier AF, Regev A. Spatial reconstruction of single-cell gene expression data. *Nat Biotechnol*. 2015;33:495–502.
- Butler A, Hoffman P, Smibert P, Papalexi E, Satija R. Integrating single-cell transcriptomic data across different conditions, technologies, and species. *Nat Biotechnol*. 2018;36:411–20.
- Young MD, Behjati S. SoupX removes ambient RNA contamination from droplet-based single-cell RNA sequencing data. *Gigascience*. 2020;9:giaa151.
- Hafemeister C, Satija R. Normalization and variance stabilization of single-cell RNA-seq data using regularized negative binomial regression. *Genome Biol*. 2019;20:296.
- Choudhary S, Satija R. Comparison and evaluation of statistical error models for scRNA-seq. *Genome Biol*. 2022;23:27.
- Tirosh I, Izar B, Prakadan SM, Wadsworth MH, Treacy D, Trombetta JJ, et al. Dissecting the multicellular ecosystem of metastatic melanoma by single-cell RNA-seq. *Science*. 2016;352:189–96.
- Zhang Z, Luo D, Zhong X, Choi JH, Ma Y, Wang S, et al. SCINA: A semi-supervised subtyping algorithm of single cells and bulk samples. *Genes*. 2019;10:531.
- Finak G, McDavid A, Yajima M, Deng J, Gersuk V, Shalek AK, et al. MAST: A flexible statistical framework for assessing transcriptional changes and characterizing heterogeneity in single-cell RNA sequencing data. *Genome Biol*. 2015;16:278.
- Korotkevich G, Sukhov V, Budin N, Shpak B, Artyomov MN, Sergushichev A. Fast gene set enrichment analysis. *BioRxiv*. February 1, 2021.

32. Efremova M, Vento-Tormo M, Teichmann SA, Vento-Tormo R. CellPhoneDB: Inferring cell-cell communication from combined expression of multi-subunit ligand-receptor complexes. *Nat Protoc.* 2020;15:1484–506.
33. Pouyababar D, Chung SW, Pezzutti OI, Perciani CT, Wang X, Ma XZ, et al. A rat liver cell atlas reveals intrahepatic myeloid heterogeneity. *iScience.* 2023;26:108213.
34. Fu X, Lin Y, Lin DM, Mechttersheimer D, Wang C, Ameen F, et al. BIDCell: Biologically-informed self-supervised learning for segmentation of subcellular spatial transcriptomics data. *Nat Commun.* 2024;15:509.
35. Lumanto P. QuPath immunofluorescence cell detection and co-localization. Protocol v1. November 13, 2023. Accessed September 12, 2025. <https://dx.doi.org/10.17504/protocols.io.e6nvwdmnwlmk/v1>
36. Collin M, McGovern N, Haniffa M. Human dendritic cell subsets. *Immunology.* 2013;140:22–30.
37. Suo C, Dann E, Goh I, Jardine L, Kleshchevnikov V, Park JE, et al. Mapping the developing human immune system across organs. *Science.* 2022;376:eabo0510.
38. Xiao M-H, Ma D, Wu S, Huang Z, Liang P, Chen H, et al. Integrative single-cell and spatial transcriptomic analyses identify a pathogenic cholangiocyte niche and TNFRSF12A as therapeutic target for biliary atresia. *Hepatology.* 2025;81:1146–63.
39. Chen D, Zheng J, Gerasimcik N, Lagerstedt K, Sjögren H, Abrahamsson J, et al. The expression pattern of the pre-B cell receptor components correlates with cellular stage and clinical outcome in acute lymphoblastic leukemia. *PLoS One.* 2016;11: e0162638.
40. Morgan D, Tergaonkar V. Unraveling B cell trajectories at single cell resolution. *Trends Immunol.* 2022;43:210–29.
41. Deczkowska A, David E, Ramadori P, Pfister D, Safran M, Li B, et al. XCR1+ type 1 conventional dendritic cells drive liver pathology in non-alcoholic steatohepatitis. *Nat Med.* 2021;27: 1043–54.
42. Shimazu R, Akashi S, Ogata H, Nagai Y, Fukudome K, Miyake K, et al. MD-2, a molecule that confers lipopolysaccharide responsiveness on Toll-like receptor 4. *J Exp Med.* 1999;189:1777–82.
43. Nakagaki BN, Mafra K, de Carvalho É, Lopes ME, Carvalho-Gontijo R, de Castro-Oliveira HM, et al. Immune and metabolic shifts during neonatal development reprogram liver identity and function. *J Hepatol.* 2018;69:1294–307.
44. Möhring T, Karch A, Falk CS, Laue T, D'Antiga L, Debray D, et al. Immune status in children before liver transplantation—A cross-sectional analysis within the ChilsSFree multicentre cohort study. *Front Immunol.* 2019;10:52.
45. Thorsen SU, Eising S, Mortensen HB, Skogstrand K, Pociot F, Johannesen J, et al. Systemic levels of CCL2, CCL3, CCL4 and CXCL8 differ according to age, time period and season among children newly diagnosed with type 1 diabetes and their healthy siblings. *Scand J Immunol.* 2014;80:452–61.
46. Zhang Y, Wu B, Zhang H, Ge X, Ying S, Hu M, et al. Inhibition of MD2-dependent inflammation attenuates the progression of non-alcoholic fatty liver disease. *J Cell Mol Med.* 2018;22: 936–47.
47. Ricciuto A, Kamath BM, Hirschfield GM, Trivedi PJ. Primary sclerosing cholangitis and overlap features of autoimmune hepatitis: A coming of age or an age-ist problem? *J Hepatol.* 2023;79:567–75.
48. Crespo M, Lappe S, Feldstein AE, Alkhoury N. Similarities and differences between pediatric and adult nonalcoholic fatty liver disease. *Metab Clin Exp.* 2016;65:1161–71.
49. Krenkel O, Hundertmark J, Abdallah AT, Kohlhepp M, Puengel T, Roth T, et al. Myeloid cells in liver and bone marrow acquire a functionally distinct inflammatory phenotype during obesity-related steatohepatitis. *Gut.* 2020;69:551–63.
50. Bhattacharyya S, Wang W, Qin W, Cheng K, Coulup S, Chavez S, et al. TLR4-dependent fibroblast activation drives persistent organ fibrosis in skin and lung. *JCI Insight.* 2018;3: e98850.

How to cite this article: Edgar RD, Nakib D, Camat D, Chung S, Lumanto P, Atif J, et al. A single-cell atlas of human pediatric liver reveals age-related hepatic gene signatures. *Hepatol Commun.* 2025;9:e0813. <https://doi.org/10.1097/HC9.0000000000000813>